

Article

# Synthesis of Various TiO<sub>2</sub> Micro-/Nano-Structures and Their Photocatalytic Performance

Anquan Deng <sup>1,2</sup> , Yufu Zhu <sup>1,\*</sup>, Xin Guo <sup>1</sup>, Lei Zhou <sup>3</sup> and Qingsong Jiang <sup>4</sup>

<sup>1</sup> Faculty of Mechanical & Material Engineering, Huaiyin Institute of Technology, Huaian 223003, China; deng\_anquan@163.com (A.D.); guoxin@hyit.edu.cn (X.G.)

<sup>2</sup> College of Material Science and Engineering, Nanjing Tech University, Nanjing 21009, China

<sup>3</sup> Faculty of Mathematics and Physics, Huaiyin Institute of Technology, Huaian 223003, China; leizhou@hyit.edu.cn

<sup>4</sup> Jiangsu Engineering Laboratory for Lake Environment Remote Sensing Technologies, Faculty of Electronic Information Engineering, Huaiyin Institute of Technology, Huaian 223003, China; jiangqingsong05@hyit.edu.cn

\* Correspondence: hyit2014@163.com; Fax: +86-517-8355-9130

Received: 29 April 2018; Accepted: 4 June 2018; Published: 12 June 2018



**Abstract:** TiO<sub>2</sub> micro-/nano-structures with different morphologies have been successfully synthesized via a hydrothermal method. The effects of the solvents on the morphology and structure of the obtained products have been studied. The objective of the present paper is to compare the photocatalytic properties of the obtained TiO<sub>2</sub> products. During the synthesis process, the tetrabutyl titanate and titanium (IV) fluoride were used as the titanium source. The obtained micro-/nano-structures were characterized by field-emission scanning electron microscopy, X-ray diffraction analysis, and nitrogen adsorption-desorption isotherms. The photocatalytic activity of the samples was evaluated by the degradation of Rhodamine B solution under simulated solar irradiation. It is found that the morphologies and structures of TiO<sub>2</sub> have a great influence on its photocatalytic activity. Compared with other samples, TiO<sub>2</sub> flower clusters assembled with nanorods exhibited a superior photocatalytic activity in the degradation of Rhodamine B.

**Keywords:** TiO<sub>2</sub>; different morphologies; photocatalytic activity; formation mechanisms

## 1. Introduction

In the past few decades, the synthesis of semiconductor micro-/nano-structures has attracted much attention in materials science communities due to the fact that this kind of material has many excellent properties, such as large specific surface area, high reactivity, strong adsorption and photocatalysis [1–4]. Among these materials, nano-TiO<sub>2</sub> semiconductor has been considered an ideal material to solve the environmental pollution problem due to its high stability, non-toxicity, and other attributes [5,6]. A large number of studies have demonstrated that there is a close relationship between the morphological characteristics and the photocatalytic efficiencies of TiO<sub>2</sub> [7–9]. By controlling the surface morphology and microstructure of TiO<sub>2</sub>, the photocatalytic performance of TiO<sub>2</sub> can be enhanced. For example, I. S. Grover et al. [8] found that the photocatalytic activity of TiO<sub>2</sub> nanotube crystals was superior to the commercial TiO<sub>2</sub> (P25), owing to its largest surface area and hollow porous surface structure.

Recently, nano-TiO<sub>2</sub> with various morphologies, including microspheres [10,11], nanosheets [12], nanorods [13], nanowires [14,15], nanotubes [15,16] and mesoporous [17], has been synthesized. Nano-TiO<sub>2</sub> with these morphologies usually has a larger specific surface area and higher degree of crystallinity [10–19]. Among the above-mentioned various TiO<sub>2</sub> micro-/nano-structures, mesoporous

TiO<sub>2</sub> has become a popular topic due to its uniform pore size, regular pore distribution and large surface area [18,20–22]. The previous studies have reported that the photocatalytic properties of mesoporous TiO<sub>2</sub> with different morphologies are quite different, and the photocatalytic activities are significantly enhanced compared with the commercial TiO<sub>2</sub> (P25) [23]. Therefore, the morphologies of TiO<sub>2</sub> should have a great influence on its photocatalytic activity. However, there have been few reports on the systematic analyses and comparisons of photocatalytic properties of TiO<sub>2</sub> with different morphologies and structures.

In this work, TiO<sub>2</sub> with various morphologies (microspheres, flower clusters assembled with nanorods, hexahedral and nanosheet structures with different morphologies) were hydrothermally synthesized by using different titanium sources under different reaction conditions. The morphologies, sizes, and elemental analysis of the synthesized samples were examined by using field emission scanning electron microscopy (FE-SEM) and X-ray diffractometer (XRD). The photocatalytic activities of obtained products were systematically studied and compared by the degradation of Rhodamine B.

## 2. Experimental Section

### 2.1. Materials

All chemicals used in this paper are of analytical grade reagents and used without further purification [24]. Titanium tetrafluoride (TiF<sub>4</sub>, 99%) was purchased from J&K Scientific Ltd. (China). Hydrochloric acid (HCl, 37%), absolute ethanol, silica spheres (50 nm), and sodium hydroxide (NaOH, 96%) were purchased from Sinopharm Chemical Reagent Co., Ltd. (China). Ionic liquid (1-butyl-2,3-dimethylimidazolium tetrafluoroborate, 97%) and tetrabutyl titanate (Ti(OC<sub>4</sub>H<sub>9</sub>)<sub>4</sub>, TBOT, 99%) were purchased from Shanghai Aladdin Bio-Chem Technology Co., Ltd. (Shanghai, China).

### 2.2. Preparation of TiO<sub>2</sub> Microspheres

In a typical synthesis, tetrabutyl titanate (TBOT) was employed as the titanium source. Primarily, 9.3 mL of absolute ethanol was mixed with 0.23 mL of HCl, followed by adding 1.3 mL of TBOT to the above mixed solution at room temperature. The whole process was carried out under the condition of magnetic stirring. After 30 min of agitation, the mixture solution was transferred to a Teflon-lined autoclave and heated at 150 °C for 4 h, then cooled down to room temperature. The final precipitate was collected by centrifugation (4000 r.p.m. for 15 min) and washed several times using absolute ethanol [25], then dried at 60 °C overnight and calcined at 400 °C for 30 min (the products were denoted as Ms). The detailed chemical reagents and reaction time used in the experiments were listed in Table 1.

**Table 1.** TiO<sub>2</sub> microspheres (Ms) samples synthesized with chemical reagents and reaction time in the experiments.

TBOT Addition (mL)	HCl Addition (mL)	Absolute Ethanol (mL)	Reaction Time (h)
1.3	0.00	9.30	4
1.3	0.03	9.30	4
1.3	0.43	9.30	4
1.3	1.50	9.30	4
1.3	0.23	4.65	4
1.3	0.23	9.30	4
1.3	0.23	18.6	4

### 2.3. Preparation of TiO<sub>2</sub> Flower Clusters Assembled with Nanorods

During the synthesis process, TBOT was also employed as the titanium source. Hydrochloric acid and deionized water (volume ratio of 1:1) were firstly mixed by magnetic stirring, and then 0.67 mL of TBOT was added to the mixed solution. 6 mg of titanium dioxide powders was sufficiently dispersed in the above mixed solution under ultrasound irradiation. Finally, the sealed Teflon-lined autoclave

containing above mixed solution was heated at 150 °C for a period of time (Table 2). The white precipitate was collected by centrifugation and washed with deionized water and absolute ethanol. Finally, the products were calcined at 400 °C for 30 min (the samples were denoted as Ns).

**Table 2.** Ns samples synthesized with chemical reagents and reaction time in the experiments.

C <sub>6</sub> H <sub>36</sub> O <sub>4</sub> Ti Addition (mL)	HCl Addition (mL)	H <sub>2</sub> O (mL)	TiO <sub>2</sub> Addition (g)	Reaction Time (h)
0.67	16	16	0.006	12
0.67	16	16	0.006	18
0.67	16	16	0.006	24
0.67	16	16	0.0	18

#### 2.4. Preparation of TiO<sub>2</sub> Hexahedral and Nanosheet Structures with Different Morphologies

Different morphologies of TiO<sub>2</sub> hexahedral and nanosheet structures could be synthesized hydrothermally using a modified version of the procedure [26–28]. 40 mM or 200 mM TiF<sub>4</sub> aqueous solution and 180 mM ionic liquid aqueous solution (1-butyl-2, 3-dimethylimidazolium tetrafluoroborate) were prepared in deionized water. 25 mL of TiF<sub>4</sub> aqueous solution was fully mixed with a certain amount of HCl, and then, 1.5 mL of ionic liquid aqueous solution (180 mM) and 0–0.325 g silica spheres were added to the mixed solution with magnetic stirring. The above solutions were transferred to a Teflon-lined autoclave and heated at 170 °C for a certain amount of time. Details describing the synthesis of the products can be found in Table 3. The obtained white precipitate was washed several times with deionized water. The silica template in the precipitate was selectively etched in aqueous 2M NaOH at 80 °C for 1 h [27]. The prepared samples were calcined at 400 °C for 30 min. The yielded products were respectively denoted as S1, S2, and S3, as demonstrated in Table 3.

**Table 3.** S1, S2, and S3 samples synthesized with chemical reagents and reaction time in the experiments.

Sample	TiF <sub>4</sub> Addition (mmol/L)	HCl Addition (μL)	Ionic Liquid Aqueous Solution (mL)	SiO <sub>2</sub> Addition (g)	Reaction Time (h)
S1	40	1000	1.5	0.325	20
S2	40	1000	1.5	0.0	20
S3	200	20	1.5	0.0	16

#### 2.5. Characterization

The morphologies of the obtained samples were examined by using field emission scanning electron microscopy (FESEM; Quanta 250 FEG, FEI, America) with an accelerating voltage of 15 kV. The samples were coated with a layer of gold by using vacuum sputtering coating machine (Q150R ES, UK) before morphological characterization. Phase analysis of the samples was recorded on a Bruker AXS Advanced X-Ray diffractometer system (XRD; D8 Advance, Bruker, Germany) in the 2θ scan range of 20–80°. N<sub>2</sub> adsorption–desorption isotherms were recorded at 77 K using a Micromeritics Tristar 3020 analyzer (Micromeritics Instrument Corp., Norcross, GA, USA).

#### 2.6. Photocatalysis Measurements

Under simulated solar irradiation, the photocatalytic measurement of the obtained samples was carried out in a 100 mL glass photoreactor. The distance between fixed intensity light source and photoreactor is 13 cm. The specific experimental procedures are as follows: 0.03 g sintered samples were added into the glass photoreactor containing 25 mL of Rhodamine B solution (10 mg L<sup>−1</sup>) and 0.5 mL of 30% of H<sub>2</sub>O<sub>2</sub>. With constant stirring, the above photoreactor was placed in the dark environment for 1 h, and then the reaction liquid was irradiated with a 300 W Xenon lamp (PLS-SXE300C, λ = 300–2500 nm, Beijing Perfectlight Technology Co., Ltd., Beijing, China). At set intervals, a small amount of reaction liquid was withdrawn and centrifuged. The obtained supernatant was preserved for the subsequent analysis. Then the absorbance of supernatant was detected at wavelengths

of 450–600 nm by an UV-visible spectrophotometer (Shimadzu UV-3600, Shimadzu corporation, Kyoto, Japan). Simultaneously, some control experiments were also carried out under the condition that only light, only  $\text{H}_2\text{O}_2$ , or only catalyst and light was applied during the photocatalytic process.

### 3. Results and Discussion

#### 3.1. Characterization of $\text{TiO}_2$ Microspheres

Compared with other structures, the microspheres have been widely concerned for its unique morphology [29]. Moreover, the pH value and solvent dosage have a great influence on the morphology of products synthesized by the hydrothermal method. In order to investigate the effect of the pH value on the morphology of  $\text{TiO}_2$  microspheres,  $\text{TiO}_2$  with different morphologies were prepared by changing the amounts of HCl in the reaction solution. The SEM images of the obtained products were shown in Figure 1. From Figure 1a, it can be clearly seen that the size of the as-obtained  $\text{TiO}_2$  microspheres are uniform and the microspheres are aggregated without the addition of HCl in the reaction solution. With increasing the amount of HCl to 0.03 mL and 0.43 mL, the microspheres with smooth surface can be obtained, and the sizes of microspheres are increased (Figure 1b,c). When 1.5 mL of HCl was added in the reaction solution, small-sized  $\text{TiO}_2$  spheres with an average diameter of approximately 500 nm were obtained, as demonstrated in Figure 1d. Based on the above results, it indicates that the amount of HCl added in the reaction solution can be used to control the morphologies and sizes of the products. With increasing HCl dosage, the hydrolysis rate of TBOT was inhibited, so the synthesized samples have good dispersibility. However, when HCl dosage in the reaction solution is too high, the growth of crystal grains will be hindered, resulting in the agglomeration of particles and reduction of size.

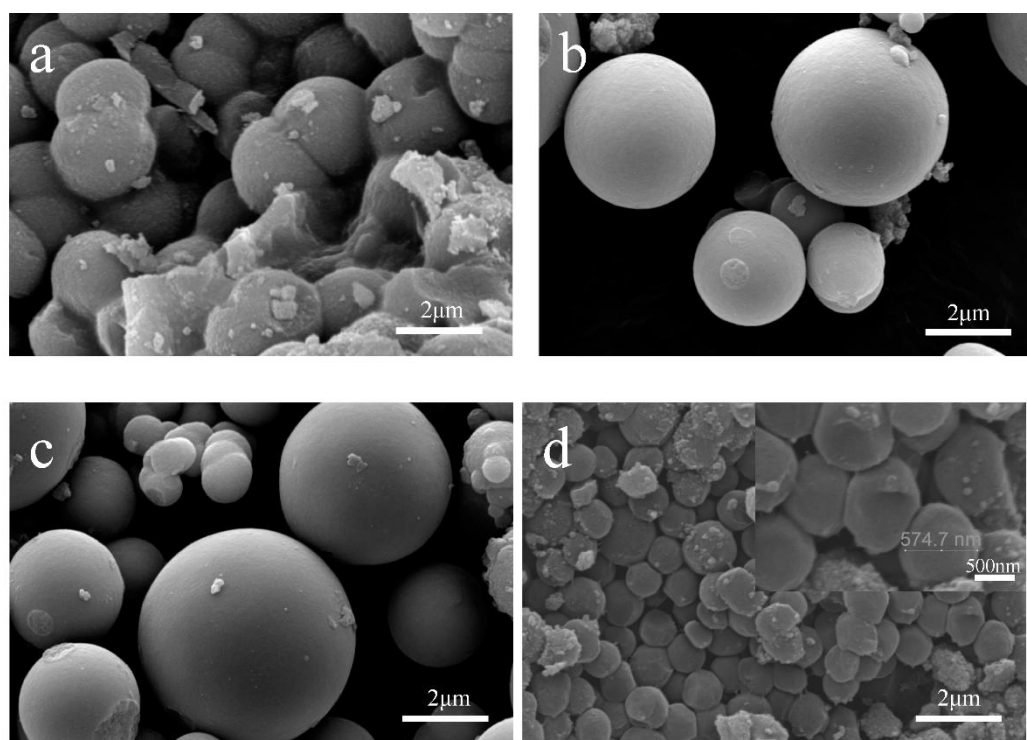


**Figure 1.** Field Emission Scanning Electron Microscopy (FESEM) images of Ms prepared with different amounts of HCl: (a) 0 mL; (b) 0.03 mL; (c) 0.43 mL and (d) 1.50 mL.

Figure 2 shows SEM images and XRD pattern of the  $\text{TiO}_2$  microspheres prepared with different amounts of absolute ethanol. When the amount of absolute ethanol was 4.65 mL,  $\text{TiO}_2$  microspheres with rough surface were obtained and the sizes of the microsphere were non-uniform (Figure 2a).

As the amounts of absolute ethanol increased, the surface of microspheres became smooth (Figure 2b). When 18.6 mL of absolute ethanol was added in the reaction solution, the size of microspheres had shrunk dramatically, and couldn't form a complete spherical structure (Figure 2c). These results show that the amount of ethanol has a great influence on the morphology of TiO<sub>2</sub> microspheres, which can be explained by the following: with increasing the amount of ethanol, the nanoparticles generated by TBOT hydrolysis are distributed uniformly in solution, forming stable and dispersive microspheres. However, an excess of ethanol added in the solution results in a relatively low concentration of Ti source, which does not allow assembling to form spherical structures, eventually resulting in the irregular aggregates shown in Figure 2c.

To further determine the crystal structure of the obtained microspheres, the phase analysis of the samples was carried out. Figure 2d shows the typical XRD pattern of the obtained microspheres. From this figure, it can be clearly seen that the diffraction peaks are consistent with the anatase TiO<sub>2</sub> (JCPDS21-1272) [30], having diffraction peaks of (101), (004), (200), (105), (211) and (204) planes at  $2\theta = 25.4^\circ$ ,  $38^\circ$ ,  $48^\circ$ ,  $54^\circ$ ,  $56^\circ$  and  $63^\circ$ , respectively. Therefore, the as-obtained samples can be determined as anatase TiO<sub>2</sub>.

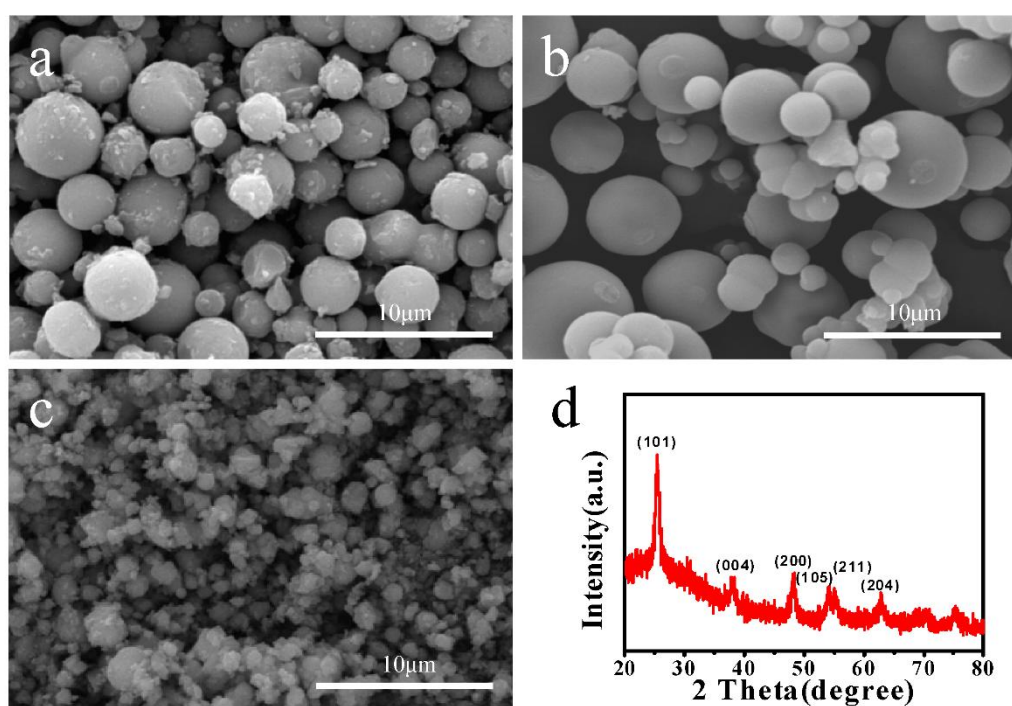
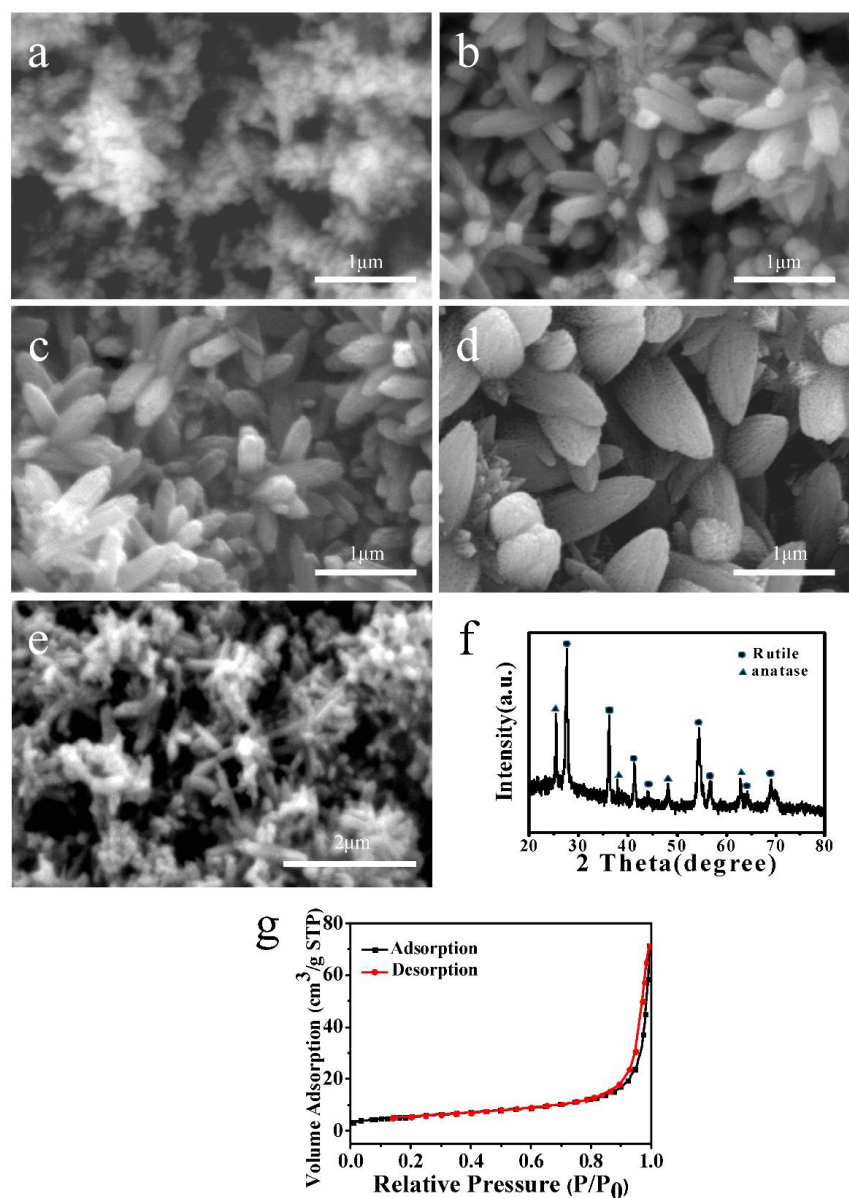


**Figure 2.** FESEM images of Ms prepared with different amounts of absolute ethanol: (a) 4.65 mL; (b) 9.30 mL and (c) 18.6 mL; (d) XRD pattern of Ms.

### 3.2. Characterization of TiO<sub>2</sub> Flower Clusters Assembled with Nanorods

The related research shows that nanorods generally exhibit larger specific surface area than microspheres. Therefore, the synthesis of TiO<sub>2</sub> flower clusters assembled with nanorods was achieved by a hydrothermal method. The formation process of the nanostructures was studied by controlling the hydrothermal reaction time and the addition of titanium dioxide powders in the reaction solution; the results are displayed in Figure 3a–d. As shown in Figure 3a, when the hydrothermal reaction was carried out for 12 h, TiO<sub>2</sub> nanorods were not fully formed. With prolonging the reaction time up to 18 h, flower-like TiO<sub>2</sub> nanostructures were formed. The average diameter and length of nanorods were approximately 300 nm and 500 nm, respectively (Figure 3b). When the reaction time was up to 24 h, the TiO<sub>2</sub> nanorods were further grown and the flower-like structure was obtained (Figure 3c). The above results indicate that the reaction time determines the morphologies of the products. Figure 3d

represents FESEM image of TiO<sub>2</sub> flower clusters assembled with nanorods prepared without the addition of titanium dioxide powders for 18 h. Compared with the SEM image shown in Figure 3b, it can be seen that the prepared nanorods became larger in size. The reason for this phenomenon is that the added titanium dioxide powders in the reaction solution acted as nucleus for crystal growth and the Ti source depleted faster than that without titanium dioxide powders, which inhibits further growth of nanoparticles, resulting in a reduction in the size of the final nanorods.



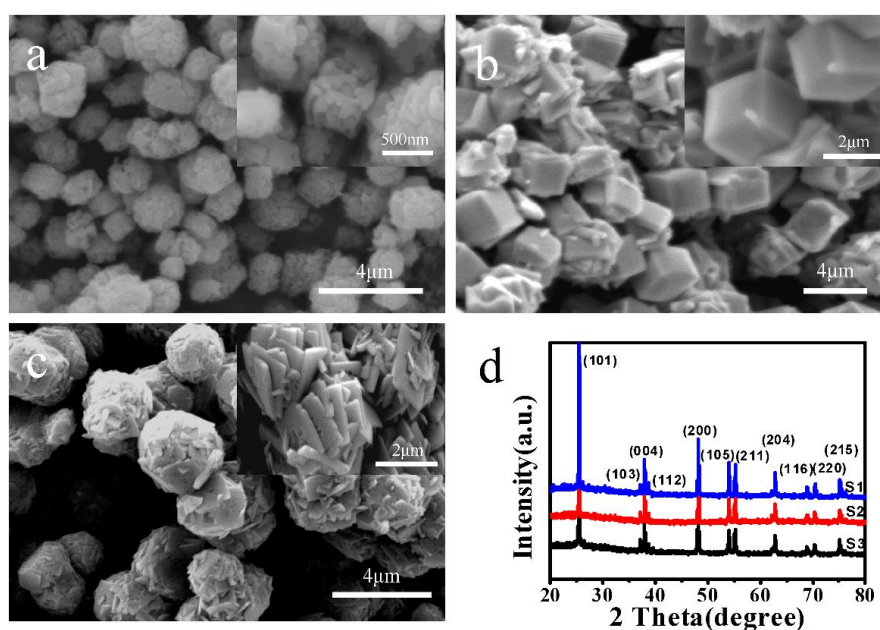
**Figure 3.** FESEM images of Ns prepared with different reaction times: (a) 12 h; (b) 18 h and (c) 24 h. (d) FESEM image of Ns prepared without the addition of titanium dioxide powders for 18 h. (e) FESEM image, (f) XRD pattern and (g) N<sub>2</sub> adsorption-desorption isotherm of Ns calcined at 400 °C.

Figure 3e is FESEM image of TiO<sub>2</sub> flower clusters assembled with nanorods calcined at 400 °C. From this figure, it can be observed that the heat treatment didn't destroy the morphology of the samples. The typical XRD pattern of the as-synthesized samples is illustrated in Figure 3f. The diffraction peaks are basically indexed to rutile TiO<sub>2</sub> (JCPDS21-1276) [31]. Furthermore, the additional peaks appear at 25.4°, 38°, 48°, and 62.8°, which can be indexed to anatase TiO<sub>2</sub>

(JCPDS21-1272). The results of XRD indicate that  $\text{TiO}_2$  flower clusters assembled with nanorods were mixed crystal of rutile and anatase. From the analysis of BET surface areas of the samples, the  $\text{N}_2$  adsorption-desorption isotherm is shown in Figure 3g. The estimated BET surface area of the samples is  $20.1 \text{ m}^2/\text{g}$ . The larger surface area and special morphology of flower-like structure together should contribute to the improved photocatalytic activity.

### 3.3. Characterization of $\text{TiO}_2$ Hexahedral and Nanosheet Structures with Different Morphologies

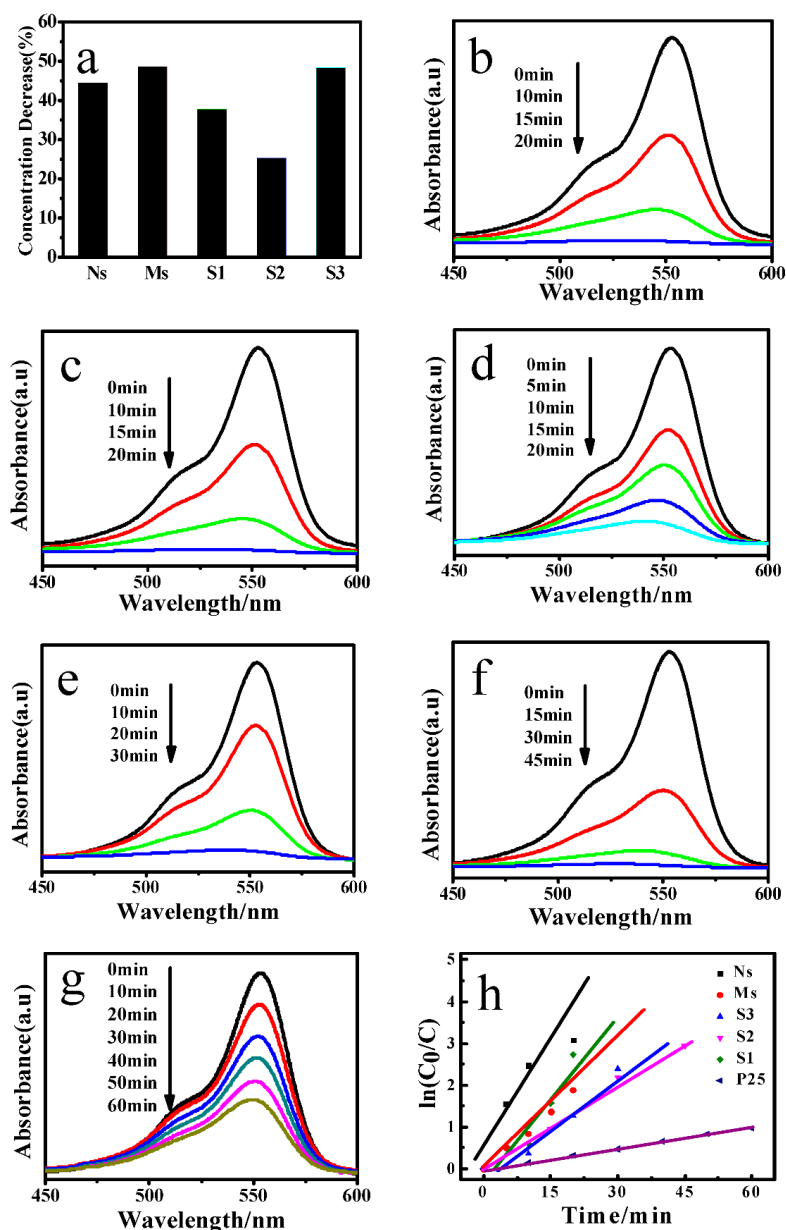
The porosity and structural properties on the surface of the samples have a certain influence on its photocatalytic performance. Hence, in order to systematically study the relationship between morphology, structure, and photocatalytic performance of  $\text{TiO}_2$ , the hydrothermal synthesis of hexahedral and nanosheet structures with different morphologies were also carried out. SEM images and XRD patterns of the samples are shown in Figure 4. S1 was hydrothermally synthesized by using silica spheres as template, which showed hexahedral structures with an average size of about 500 nm. The surface was very rough and presented numerous striped porous structures (Figure 4a). Its formation mechanism can be interpreted as follows: during the hydrothermal reaction process, the hydrolysis of  $\text{TiF}_4$  was carried out. The generated  $\text{TiO}_2$  nanoparticles were deposited randomly on the surface of the  $\text{SiO}_2$  templates. After the templates were etched by sodium hydroxide aqueous solution, the porous structures as demonstrated in Figure 4a were formed. S2 was hexahedral structures with a side length of about  $2 \mu\text{m}$ , which was prepared without the addition of  $\text{SiO}_2$  templates (Figure 4b). Compared with S1 (Figure 4a), microstructures with relatively smoother surfaces were obtained. Figure 4c presents the low- and high-magnification SEM images of the as-prepared S3. From this figure, it can be clearly observed that  $\text{TiO}_2$  microspheres were composed of a number of self-assembled crystal nanosheets with a thickness of approximately 100 nm. Compared with the preparation condition of S2, the new crystal began to nucleate and grow on the nanosheets due to the increased concentration of  $\text{TiF}_4$ . As the hydrothermal reaction proceeded, more nanosheets were produced, and finally, the self-assembled  $\text{TiO}_2$  microspheres with nanosheets were obtained. Figure 4d shows the XRD patterns of S1, S2, and S3. Obviously, there were similar diffraction patterns and sharp diffraction peaks. The diffraction peaks were highly consistent with that of anatase  $\text{TiO}_2$  (JCPDS21-1272).



**Figure 4.** FESEM images of  $\text{TiO}_2$  hexahedral and nanosheet structures with different morphologies: (a) S1; (b) S2 and (c) S3; (d) XRD patterns of S1, S2, and S3.

### 3.4. Photocatalysis Measurement

Simulated-sunlight-induced photocatalytic degradation of Rhodamine B solution was performed to evaluate the photocatalytic activity of Ns, Ms, S1, S2, and S3. To explore adsorption properties of the samples for Rhodamine B, the obtained Ns, Ms, S1, S2 and S3 were added in the Rhodamine B solution and placed in dark for 1 h before illumination. As shown in Figure 5a, the adsorption properties of Ns, Ms, S1, S2 and S3 were different. The adsorption rates for Ns, Ms, S1, S2 and S3 were 44.36%, 48.57%, 37.78%, 25.25%, and 48.27%, respectively. Among them, Ms exhibited the best adsorption properties ( $Ms > S3 > Ns > S1 > S2$ ). This indicates that the morphologies and structures of the  $TiO_2$  affect the adsorption properties of the obtained products.



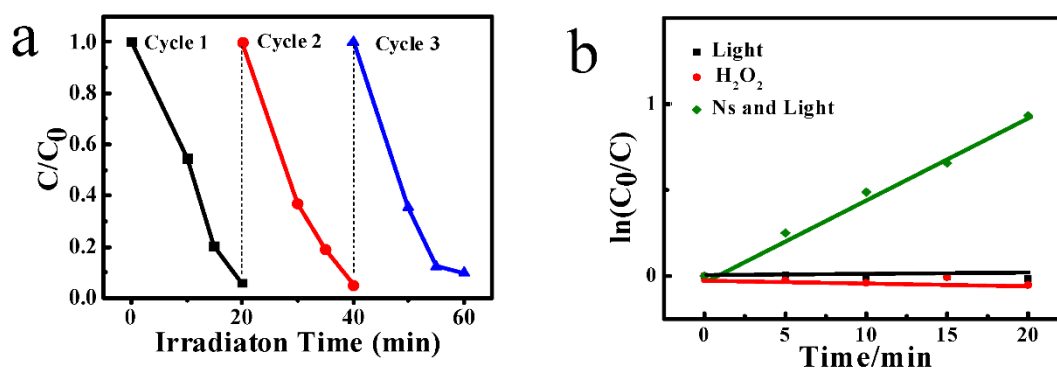
**Figure 5.** (a) The concentration decreases of Rhodamine B (RhB) aqueous solution in dark for 1 h before illumination; UV-vis spectra of (b) Ns; (c) S1; (d) Ms; (e) S3; (f) S2; (g) P25; and (h) kinetics of RhB degradation over samples.



Figure 5b–g displays UV-vis spectra of Rhodamine B solution degraded by the samples. From these figures, the decrease in absorbance of Rhodamine B solution can be clearly observed along with increasing the irradiation time. In addition, compared with P25, the whole processes of photocatalytic degradation of the synthesized samples were completed in a relatively short period of time.

In order to compare the photocatalytic performances of the obtained samples more intuitively, based on UV-vis spectra displayed in Figure 5b–g, the kinetics of Rhodamine B photo-degradation over Ns, Ms, S1, S2, S3, and P25 are given in Figure 5h. The  $k$  and  $C_0/C$  represent the degradation reaction rate in  $\text{min}^{-1}$  and the normalized Rhodamine B concentration, respectively [32]. Through the analysis of the kinetics, one can draw a conclusion that the order of the degradation reaction rate is listed below: Ns ( $k = 0.183$ ) > S1 ( $k = 0.145$ ) > Ms ( $k = 0.106$ ) > S3 ( $k = 0.082$ ) > S2 ( $k = 0.065$ ) > P25 ( $k = 0.016$ ). The results explicitly indicate that Ns have best degradation performance. Therefore, the Ns are the more suitable catalyst for the degradation of Rhodamine B.

The catalytic longevity of the catalysts was also studied, and the results are shown in Figure 6a. After three cycles of degradation of Rhodamine B solution, the degradation rate of Ns is still very high. It thus demonstrates that the obtained catalysts possess excellent catalytic longevity. In order to investigate the influence of light and  $\text{H}_2\text{O}_2$  on the degradation performance of the catalysts, a series of controlled catalytic experiments were performed. As shown in Figure 6b, it can be seen that no degradation of Rhodamine B can be observed under the condition that only light or  $\text{H}_2\text{O}_2$  was applied during the photocatalytic process. When light and Ns was simultaneously applied, the degradation of Rhodamine B took place. The degradation rate is lower than that of the solution containing Ns and  $\text{H}_2\text{O}_2$  (Figure 5h). From the above experimental results, it can be concluded that synergistic effects of Ns, light and  $\text{H}_2\text{O}_2$  contributed to the enhanced degradation efficiency.



**Figure 6.** (a) Cyclic degradation efficiency of Ns under simulated solar irradiation; (b) The effect of light and  $\text{H}_2\text{O}_2$  on the degradation efficiency of the catalyst.

#### 4. Conclusions

$\text{TiO}_2$  with different morphologies were successfully synthesized by a facile hydrothermal method. The XRD results indicate that  $\text{TiO}_2$  flower clusters assembled with nanorods are of a mixed crystal phase consisting of rutile and anatase. The other synthesized  $\text{TiO}_2$  nanostructures are anatase. Based on the photocatalytic tests, it can be seen that all as-prepared samples have good photocatalytic performance. Among these samples,  $\text{TiO}_2$  flower clusters assembled with nanorods exhibit superior photocatalytic activity. The order of photocatalytic efficiencies of samples is as follows, Ns > S1 > Ms > S3 > S2, indicating that the morphologies and structures of  $\text{TiO}_2$  have a great influence on its photocatalytic activity.

**Author Contributions:** A.D. conceived the experiments, directed the study, and analyzed the data. Q.J. carried out optical spectroscopy experiments. The whole team contributed in writing up the manuscript.

**Funding:** This research was funded by the Natural Science Foundation of Jiangsu Province (grant nos. BK20161300, BK20161303, BK20150418), the Six Talent Peaks Project in Jiangsu Province (Grant nos. XNY-008, DZXX-011) and also sponsored by Qing Lan Project and 333 Project of Jiangsu Province.

**Conflicts of Interest:** The authors declare no conflict of interest.

## References

1. Luo, L.; Qiao, H.; Chen, K.; Fei, Y.Q.; Wei, Q.F. Fabrication of electrospun ZnMn<sub>2</sub>O<sub>4</sub> nanofibers as anode material for lithium-ion batteries. *Electrochim. Acta* **2015**, *177*, 283–289. [[CrossRef](#)]
2. Liu, H.; Li, W.; Shen, D.K.; Zhao, D.Y.; Wang, G.X. Graphitic carbon conformal coating of mesoporous TiO<sub>2</sub> hollow spheres for high-performance lithium ion battery anodes. *J. Am. Chem. Soc.* **2015**, *137*, 13161–13166. [[CrossRef](#)] [[PubMed](#)]
3. Wang, L.G.; Zheng, D.P.; Zhang, S.P.; Cui, H.Z.; Li, D.X. Effect of nano-SiO<sub>2</sub> on the hydration and microstructure of Portland cement. *Nanomaterials* **2016**, *6*, 241. [[CrossRef](#)] [[PubMed](#)]
4. Li, J.; Yu, Y.; Zhang, L.Z. Bismuth oxyhalide nanomaterials: Layered structures meet photocatalysis. *Nanoscale* **2014**, *6*, 8473–8488. [[CrossRef](#)] [[PubMed](#)]
5. Nguyen, V.M.; Li, W.L.; Pham, V.H.; Wang, L.J.; Sheng, P.T.; Cai, Q.Y.; Grimes, C. A CdS/ZnSe/TiO<sub>2</sub> nanotube array and its visible light photocatalytic activities. *J. Colloid Interface Sci.* **2016**, *462*, 389–396. [[CrossRef](#)] [[PubMed](#)]
6. Dong, S.S.; Dong, S.S.; Zhou, D.D.; Zhou, X.; Ma, D.M.; Du, Y.L. Synthesis of Er<sup>3+</sup>: Al<sub>2</sub>O<sub>3</sub>-doped and rutile-dominant TiO<sub>2</sub> composite with increased responsive wavelength range and enhanced photocatalytic performance under visible light irradiation. *J. Mol. Catal. A Chem.* **2015**, *407*, 38–46. [[CrossRef](#)]
7. Chen, X.B.; Mao, S.S. Titanium dioxide nanomaterials: Synthesis, properties, modifications, and applications. *Chem. Rev.* **2007**, *107*, 2891–2959. [[CrossRef](#)] [[PubMed](#)]
8. Grover, I.S.; Singh, S.; Pal, B. The preparation, surface structure, zeta potential, surface charge density and photocatalytic activity of TiO<sub>2</sub> nanostructures of different shapes. *Appl. Surf. Sci.* **2013**, *280*, 366–372. [[CrossRef](#)]
9. Yang, H.G.; Liu, G.; Qiao, S.Z.; Sun, C.H.; Jin, Y.G.; Smith, S.C.; Zou, J.; Cheng, H.M.; Lu, G.Q. Solvothermal synthesis and photoreactivity of anatase TiO<sub>2</sub> nanosheets with dominant {001} facets. *J. Am. Chem. Soc.* **2009**, *131*, 4078–4083. [[CrossRef](#)] [[PubMed](#)]
10. Duan, Y.D.; Fu, N.Q.; Fang, Y.Y.; Li, X.; Liu, Q.; Zhou, X.; Lin, Y. Synthesis and formation mechanism of mesoporous TiO<sub>2</sub> microspheres for scattering layer in dye-sensitized solar cells. *Electrochim. Acta* **2013**, *113*, 109–116. [[CrossRef](#)]
11. Li, Z.Q.; Ding, Y.; Mo, L.E.; Hu, L.H.; Wu, J.H.; Dai, S.Y. Fine tuning of nanocrystal and pore sizes of TiO<sub>2</sub> submicrospheres toward high performance dye-sensitized solar cells. *ACS Appl. Mater. Interfaces* **2015**, *7*, 22277–22283. [[CrossRef](#)] [[PubMed](#)]
12. Dozzi, M.V.; Selli, E. Specific facets-dominated anatase TiO<sub>2</sub>: Fluorine-mediated synthesis and photoactivity. *Catalysts* **2013**, *3*, 455–485. [[CrossRef](#)]
13. Shalan, A.E.; Rashad, M.M.; Yu, Y.H.; Lira-Cantú, M.; Abdel-Mottaleb, M.S.A. A facile low temperature synthesis of TiO<sub>2</sub> nanorods for high efficiency dye sensitized solar cells. *Appl. Phys. A* **2013**, *110*, 111–122. [[CrossRef](#)]
14. Li, H.Y.; Lu, W.B.; Tian, J.Q.; Luo, Y.L.; Asiri, A.M.; Al-Youbi, A.O.; Sun, X. Synthesis and study of plasmon-induced carrier behavior at Ag/TiO<sub>2</sub> nanowires. *Chem. Eur. J.* **2012**, *18*, 8508–8514. [[CrossRef](#)] [[PubMed](#)]
15. Yuan, Z.Y.; Su, B.L. Titanium oxide nanotubes, nanofibers and nanowires. *Colloids Surf. A Physicochem. Eng. Asp.* **2004**, *241*, 173–183. [[CrossRef](#)]
16. Bao, Z.Q.; Xie, H.X.; Zhu, Q.; Qian, J.S.; Ruan, P.; Zhou, X.F. Microsphere assembly of TiO<sub>2</sub> with tube-in-tube nanostructures: Anisotropic etching and photovoltaic enhancement. *CrystEngComm* **2013**, *15*, 8972–8976. [[CrossRef](#)]
17. Ahirwar, D.; Bano, M.; Khan, F. Synthesis of mesoporous TiO<sub>2</sub> and its role as a photocatalyst in degradation of indigo carmine dye. *J. Sol-Gel Sci. Technol.* **2016**, *79*, 228–237. [[CrossRef](#)]
18. Yu, J.G.; Yu, H.G.; Cheng, B.; Zhao, X.J.; Zhang, Q.J. Preparation and photocatalytic activity of mesoporous anatase TiO<sub>2</sub> nanofibers by a hydrothermal method. *J. Photochem. Photobiol. A* **2006**, *182*, 121–127. [[CrossRef](#)]

19. Bian, Z.F.; Zhu, J.; Cao, F.L.; Huo, Y.N.; Lu, Y.F.; Li, H.X. Solvothermal synthesis of well-defined TiO<sub>2</sub> mesoporous nanotubes with enhanced photocatalytic activity. *Chem. Commun.* **2010**, *46*, 8451–8453. [[CrossRef](#)] [[PubMed](#)]
20. Li, X.; Liu, P.W.; Mao, Y.; Xing, M.Y.; Zhang, J.L. Preparation of homogeneous nitrogen-doped mesoporous TiO<sub>2</sub> spheres with enhanced visible-light photocatalysis. *Appl. Catal. B Environ.* **2015**, *164*, 352–359. [[CrossRef](#)]
21. Li, W.; Wu, Z.X.; Wang, J.X.; Elzatahry, A.A.; Zhao, D.Y. A perspective on mesoporous TiO<sub>2</sub> materials. *Chem. Mater.* **2013**, *26*, 287–298. [[CrossRef](#)]
22. Guo, C.S.; Xu, J.; Zhang, Y.; He, Y. Hierarchical mesoporous TiO<sub>2</sub> microspheres for the enhanced photocatalytic oxidation of sulfonamides and their mechanism. *RSC Adv.* **2012**, *2*, 4720–4727. [[CrossRef](#)]
23. He, F.; Li, J.L.; Li, T.; Li, G.X. Solvothermal synthesis of mesoporous TiO<sub>2</sub>: The effect of morphology, size and calcination progress on photocatalytic activity in the degradation of gaseous benzene. *Chem. Eng. J.* **2014**, *237*, 312–321. [[CrossRef](#)]
24. Wang, J.; Zhou, Y.K.; Hu, Y.Y.; O’Hayre, R.; Shao, Z.P. Facile synthesis of nanocrystalline TiO<sub>2</sub> mesoporous microspheres for lithium-ion batteries. *J. Phys. Chem. C* **2011**, *115*, 2529–2536. [[CrossRef](#)]
25. Chi, B.; Zhao, L.; Jin, T. One One-step template-free route for synthesis of mesoporous N-doped titania spheres. *J. Phys. Chem. C* **2007**, *111*, 6189–6193. [[CrossRef](#)]
26. Crossland, E.J.W.; Noel, N.; Sivaram, V.; Leijtens, T.; Alexander-Webber, J.A.; Snaith, H.J. Mesoporous TiO<sub>2</sub> single crystals delivering enhanced mobility and optoelectronic device performance. *Nature* **2013**, *495*, 215–219. [[CrossRef](#)] [[PubMed](#)]
27. Niu, J.A.; Shen, S.S.; Zhou, L.; Liu, Z.S.; Feng, P.Z.; Ou, X.M.; Qiang, Y.H. Synthesis and hydrogenation of anatase TiO<sub>2</sub> microspheres composed of porous single crystals for significantly improved photocatalytic activity. *RSC Adv.* **2016**, *6*, 62907–62910. [[CrossRef](#)]
28. Niu, J.A.; Shen, S.S.; He, S.F.; Liu, Z.; Feng, P.; Zhang, S.; Ou, X.M.; Qiang, Y.H.; Zhu, Z. Synthesis and photoactivity of anatase porous single crystals with different pore sizes. *Ceram. Int.* **2015**, *41*, 11936–11944. [[CrossRef](#)]
29. Ma, S.L.; Zhan, S.H.; Jia, Y.N.; Zhou, Q.X. Superior Antibacterial Activity of Fe<sub>3</sub>O<sub>4</sub>-TiO<sub>2</sub> Nanosheets under Solar Light. *ACS Appl. Mater. Interfaces* **2015**, *7*, 21875–21883. [[CrossRef](#)] [[PubMed](#)]
30. Liu, S.Q.; Zhang, N.; Tang, Z.R.; Xu, Y.J. Synthesis of one-dimensional CdS@TiO<sub>2</sub> core-shell nanocomposites photocatalyst for selective redox: The dual role of TiO<sub>2</sub> shell. *ACS Appl. Mater. Interfaces* **2012**, *4*, 6378–6385. [[CrossRef](#)] [[PubMed](#)]
31. Gao, Q.; Wu, X.M.; Fan, Y.M.; Zhou, X.Y. Fabrication of hierarchically structured rutile TiO<sub>2</sub> nanorods on mica particles and their superhydrophilic coating without UV irradiation. *Appl. Surf. Sci.* **2014**, *289*, 281–288. [[CrossRef](#)]
32. Zhu, Z.F.; Yan, Y.; Li, J.Q. One-step synthesis of flower-like WO<sub>3</sub>/Bi<sub>2</sub>WO<sub>6</sub> heterojunction with enhanced visible light photocatalytic activity. *J. Mater. Sci.* **2016**, *51*, 2112–2120. [[CrossRef](#)]

